



Universidad Autónoma
de Madrid

Biblos-e Archivo
Repositorio Institucional UAM

Repositorio Institucional de la Universidad Autónoma de Madrid

<https://repositorio.uam.es>

Esta es la **versión de autor** del artículo publicado en:
This is an **author produced version** of a paper published in:

IEEE Transactions on Antennas and Propagation 69.11 (2021): 8003 - 8008

DOI: <https://doi.org/10.1109/TAP.2021.3083790>

Copyright: © 2021 IEEE

El acceso a la versión del editor puede requerir la suscripción del recurso

Access to the published version may require subscription

Communication

Degeneracy-discriminating modal FEM computation in higher-order rotationally symmetric waveguides

Gines Garcia-Contreras, Juan Córcoles, *Senior Member, IEEE*, and Jorge A. Ruiz-Cruz, *Senior Member, IEEE*

Abstract—An accurate and efficient method is proposed to characterize waveguides with arbitrary cross-sections exhibiting discrete rotational symmetries, known in the literature as C_N symmetries. This new method is based on a novel tailored 2D Finite Element Method (FEM) formulation exploiting rotationally periodic boundary conditions involved in the minimum sector that defines the waveguide cross-section. While retaining the proven accuracy and convergence rate of FEM, it allows for a reduction of dimensionality of the problem and classifies the modes with respect to their rotational symmetry.

Most importantly, it discriminates reliably and unambiguously degenerate modes (no matter how high their order is) with the exact same computed cutoff frequency value. This is especially interesting in modal analysis of devices involving circular polarization, since the formulation inherently provides different mode sets for clockwise and counterclockwise circularly polarized modes. The method has been tested on a wide variety of waveguides and computed higher-order modes have been compared against analytical solutions and general-purpose FEM.

Index Terms—Finite element methods, waveguide theory, circular polarization, TE modes, TM modes, rotational symmetry, C_N devices.

I. INTRODUCTION

RECENTLY, the analysis of higher-order symmetries (twist, glide, rotation...) in transmission media problems has regained the attention of the scientific community because of its prospective application to the analysis of a wide variety of devices [1], [2]. This has motivated researchers to further study how these geometrical properties influence the electromagnetic propagation in higher-order symmetrical devices in an attempt to facilitate their analysis and to provide tools for a better understanding of their nature. Higher-order symmetry analysis, which typically relies on modal expansions and classification, can be studied either from a longitudinal (e.g. using Floquet or Bloch modes [3], [4]) or transversal perspective [5]. In waveguide devices, characterization of the modal spectrum is the starting point of any design, and, for many analysis techniques [6]–[8], it is crucial to compute efficiently and precisely a high number of modes classified by their modal symmetries.

To cope with arbitrarily shaped cross-sections, there are long-known numerical methods to compute modes in homogeneous waveguides [9], [10], such as the two-dimensional Finite

Element Method (2D-FEM) [7], [11], [12], Generalized Transverse Resonance (GTR) [13], Boundary Integral-Resonant Mode Expansion (BI-RME) [6], [14] and Boundary Contour Mode-Matching Methods (BCMM) [15]–[17]. However, a non tailored application of these methods has some problems when dealing with structures with higher-order symmetries, as they inherently have sets of degenerate modes that may generate discrepancies in their computation. This has an impact when analysing devices intended to work with a specific polarisation (e.g. circular [18]), as the desired modes may have to be derived as a combination of two degenerate modes with a different kind of polarisation. The problem arises when the method used to obtain their cutoff frequencies involves any kind of approximation, as is always the case, and thus the need of manually checking and identifying degeneracy appears.

Symmetries have typically been exploited in both analytical and numerical methods to improve accuracy of results or performance [6], [19], mainly axial symmetry, which allows for a dimensionality reduction of up to 4 (as in Fig. 1(a)). The main objective of this paper is translating these strategies to the discrete rotational C_N [20] symmetry by an angle of $2\pi/N$ radians, where N is a positive integer. This C_N symmetry appears in many state-of-the-art devices, especially those dealing with circular polarization [21] such as polarisers, field rotators or antenna apertures [2], [7], [8], [18], [22], [23]. It defines $2\pi/N$ as the radians a structure needs to be turned along its rotational axis to obtain an identical cross section as the one prior to the rotation (see the cross-section in Fig. 1(b)). Identifying and taking advantage of this property allows for an alternative, complete set of modes to be obtained that fulfil a rotational symmetry boundary condition, and can thus be computed by simulating a wedge of the structure instead of its entirety [5].

This work proposes a robust and dedicated FEM formulation to efficiently compute modes in C_N structures for an arbitrary positive integer N . Its main advantage is the unambiguous and accurate identification of degenerate modes. Therefore, it is not necessary to manually build circularly polarized modes from other linearly polarized ones. Other key benefits of the proposed method are the great reduction of the dimensionality of the problem proportional to the value of N , and its ability to predict and classify the modes of the structure based on their rotational symmetry.

II. PROBLEM FORMULATION

A. C_N rotationally symmetric homogeneous waveguides

The complete set of TE and TM modes, for a homogeneous waveguide enclosed by a perfect metallic conductor with a

This work was supported by the Spanish Government (Agencia Estatal de Investigación, Fondo Europeo de Desarrollo Regional) (AEI/FEDER, UE) under Grant TEC2016-76070-C3-1-R (ADDMATE).

G. Garcia-Contreras, J. Córcoles, and J. A. Ruiz-Cruz are with the Department of Electronic and Communication Technology, Escuela Politécnica Superior, Universidad Autónoma de Madrid, 28049 Madrid, Spain (e-mail: gines.garcia@uam.es).

Manuscript received January 7th, 2021; revised March 5th, 2021.

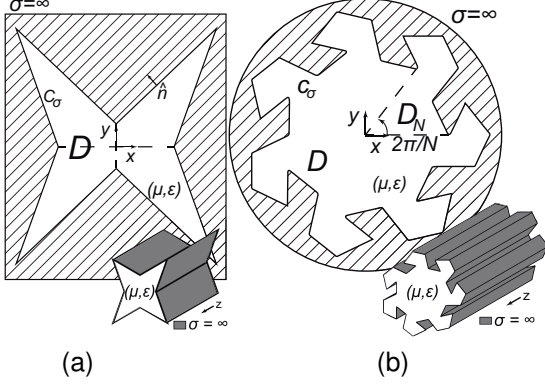


Fig. 1. (a) Generic cross-section with two-fold axial symmetry (also with C_2 symmetry in the example). (b) Generic C_N cross-section (C_7 in the plotted example, with no planes of axial symmetry) and one of the possible domains D_N to be used for its mode spectrum characterization by the proposed formulation.

generic cross-section D , is obtained from the eigensolutions (ψ, k_c^2) of the scalar 2D Helmholtz equation $\Delta\psi + k_c^2\psi = 0$ with the following boundary conditions:

$$\left. \frac{\partial\psi}{\partial n} \right|_{c_\sigma} = 0 \quad \text{for TE modes,} \quad (1)$$

$$\psi|_{c_\sigma} = 0 \quad \text{for TM modes,} \quad (2)$$

where \hat{n} is the direction normal to the contour c_σ of the cross-section, and k_c is the cutoff wavenumber for each mode. The total electromagnetic field is obtained from ψ by using classic expressions [24], [25], since ψ represents the longitudinal magnetic field H_z for TE modes and the longitudinal electric field E_z for TM modes, without the complex exponential variation along the propagation direction z . The TE and TM modes of closed and homogeneous waveguides with C_N symmetry can be made to satisfy the following equation, which shows a relationship in cylindrical coordinates between slices of the same angular width in their cross-section, given a cylindrical reference system (ρ, φ, z) (polar when omitting the z -variation) fixed on the circumcenter of the structure [20]:

$$\psi(\rho, \varphi + \frac{2\pi}{N}) = e^{-j\frac{2\pi}{N}q} \psi(\rho, \varphi). \quad (3)$$

The variable q is an integer that can be defined in the range $[-N/2] < q \leq [N/2]$, where $[\cdot]$ represents the floor function. Defining q within these limits allows for an intuitive way of obtaining degenerated modes, the reason for this being that if a value of q is found that satisfies the equation (3), then the value $-q$ will satisfy it as well and the fields obtained in both solutions will be complex conjugates [20]. The value of q will be referred to as “mode class” since it determines the family of modes that will be derived, in an analogous way of the sets that appear when enforcing perfect electric and/or magnetic conductor (PEC/PMC, respectively) in axial symmetry planes.

The relationship in (3) shows that to obtain the modes of a structure with rotational symmetry of order N it is only needed to analyse a wedge D_N of $2\pi/N$ radians, thus reducing N times the domain. This well-known result [5], [19] will be

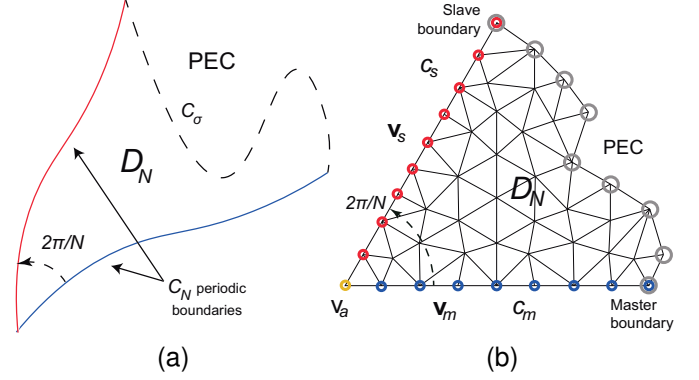


Fig. 2. (a) Problem definition and (b) generic FEM implementation

further revisited in this paper to propose a novel specific FEM-based formulation for this problem, exploiting the concept of rotational periodic boundary conditions in the cross-section contour. An example of a C_7 waveguide cross-section is shown in Fig. 1(b), with a possible reduced domain D_7 that could be employed to compute the modes using this method.

B. C_N -FEM modal computation

When working with FEM a solution for ψ is sought with the form:

$$\psi = \sum_{i=1}^{N_{dof}} v^{(i)} \phi^{(i)}, \quad (4)$$

where $v^{(i)}$ (arranged in column vector \mathbf{v}) are the degrees of freedom (DOFs), $\phi^{(i)}$ the basis functions and N_{dof} the total number of DOFs in the problem. In (4) coordinate dependence (ρ, φ) is omitted for the sake of clarity (and will be implicit from here on). To obtain TE and TM modes one can solve the discretized generalized eigenvalue problem $(\mathbf{S} - k_c^2 \mathbf{T})\mathbf{v} = \mathbf{0}$ derived from the weak form of the Helmholtz equation [11] with the PEC conditions (1) or (2) enforced by computing the FEM matrices \mathbf{S} and \mathbf{T} in the full domain $\Omega = D$, with entries:

$$S^{(i,j)} = \iint_{\Omega} \nabla_t \phi^{(i)} \cdot \nabla_t \phi^{(j)} d\Omega \quad [N_{dof} \times N_{dof}], \quad (5)$$

$$T^{(i,j)} = \iint_{\Omega} \phi^{(i)} \phi^{(j)} d\Omega \quad [N_{dof} \times N_{dof}]. \quad (6)$$

The C_N symmetry can be exploited to reduce the original computational domain to just a fraction of it, so that $\Omega = D_N$. The expression presented in (3) allows for a very loose formulation of the C_N problem, such as the one shown in Fig. 2(a). Periodic boundaries can be chosen arbitrarily and may be curvilinear, as long as the angular gap between curves is $2\pi/N$ rad. The remaining edges of the structure must have the PEC boundary conditions in (1) or (2) for closed waveguide.

Taking this into account, a more specific sketch designed for FEM simulation is presented in Fig. 2(b), which shows a slice of a generic C_N cross-section with straight boundaries for rotational symmetry, different from Fig 2(a) but without loss of generality, by assuming, for the sake of simplicity and only for visualization purposes, triangular elements with first-order interpolatory polynomial functions. It is possible

to identify the DOFs for the nodes in the edges of the structure, in this case arranged in vector \mathbf{v}_m for the nodes in the lower or *main* [26], [27] boundary c_m , vector \mathbf{v}_s for the nodes in the contour angularly shifted $2\pi/N$ radians from the reference, i.e. *secondary* boundary c_s , and v_a for the node at the rotational axis. Please note that, at the mesh level, the number of elements in c_m and in c_s are not restricted by any relation, i.e. boundary meshes need not match. That said, to avoid introducing geometrical errors due to curved boundaries, main and secondary boundaries are set as straight lines, as this is always possible for any C_N cross-section. In the remaining edge nodes, including the nodes that belong to both the conductor and the periodic boundaries, PEC boundary conditions have to be applied. We can define the desired function in these facets and establish the relationship between them according to (3):

$$\psi_m = \sum_{i=1}^M v_m^{(i)} \phi_m^{(i)} \quad \text{in } c_m, \quad \psi_s = \sum_{i=1}^S v_s^{(i)} \phi_s^{(i)} \quad \text{in } c_s, \quad (7)$$

$$\sum_{i=1}^S v_s^{(i)} \phi_s^{(i)} = \sum_{i=1}^M v_m^{(i)} \phi_m^{(i)} e^{-\frac{j2\pi q}{N}}, \quad (8)$$

where S and M are the total number of nodes at the secondary and main boundaries, respectively. Note that in this expression every $\phi_m^{(i)}$ is first projected onto c_s . There will be R remaining nodes in the system, so that $N_{dof} = R + S + M + 1$ (the last term accounting for the node at the rotational axis). A Galerkin approach can be applied to (8) to seek the relationship between \mathbf{v}_s and \mathbf{v}_m :

$$\int_{c_s} \phi_s^{(j)} \sum_{i=1}^S v_s^{(i)} \phi_s^{(i)} dl = \int_{c_s} \phi_s^{(j)} \sum_{i=1}^M v_m^{(i)} \phi_m^{(i)} e^{-\frac{j2\pi q}{N}} dl. \quad (9)$$

We can obtain the final relationship to be used in the numerical implementation by arranging (9) in matrix form with column vectors \mathbf{v}_s and \mathbf{v}_m :

$$\mathbf{v}_s = e^{-\frac{j2\pi q}{N}} \mathbf{P}_{ss}^{-1} \mathbf{P}_{sm} \mathbf{v}_m, \quad (10)$$

where the real matrices \mathbf{P}_{ss} and \mathbf{P}_{sm} have the following entries with indices i, j :

$$P_{ss}^{(i,j)} = \int_{c_s} \phi_s^{(i)} \phi_s^{(j)} dl \quad [S \times S], \quad (11)$$

$$P_{sm}^{(i,j)} = \int_{c_s} \phi_s^{(i)} \phi_m^{(j)} dl \quad [S \times M]. \quad (12)$$

Note that if the nodes are radially aligned (i.e. are at the same radial distance from the node corresponding to v_a) $\mathbf{P}_{ss}^{-1} \mathbf{P}_{sm} = \mathbf{I}_M$, where \mathbf{I}_M refers to an identity matrix of dimensions $M \times M$. It is now possible to display the relationship between all the DOFs in the system such as the one presented in Fig. 2(b) and its reduced version without the DOFs at the secondary boundary, in a similar fashion as the one proposed in [12] for linearly-shifted periodic boundary conditions used to analyse structures under Floquet-mode excitation:

$$\begin{bmatrix} \mathbf{v}_r \\ \mathbf{v}_m \\ v_a \\ \mathbf{v}_s \end{bmatrix} = \begin{bmatrix} \mathbf{I}_R & \mathbf{0} & \mathbf{0} \\ \mathbf{0} & \mathbf{I}_M & \mathbf{0} \\ \mathbf{0} & \mathbf{0} & e^{-\frac{j2\pi q}{N}} \\ \mathbf{0} & e^{-\frac{j2\pi q}{N}} \mathbf{P}_{ss}^{-1} \mathbf{P}_{sm} & \mathbf{0} \end{bmatrix} \begin{bmatrix} \mathbf{v}_r \\ \mathbf{v}_m \\ v_a \end{bmatrix} = \mathbf{P} \tilde{\mathbf{v}} \quad (13)$$

Here, the subscripts a , m and r refer respectively to the DOFs corresponding to the node at the rotation axis, the nodes at the main boundary facet and the remaining nodes of the system. The final number of unknowns is $R + M + 1$. Node v_a requires a special treatment since it actually belongs to both periodic facets, and for that reason has to be present in the reduced system, although it can be removed for $q \neq 0$. This complex matrix \mathbf{P} of size $[N_{dof} \times (R + M + 1)]$ is utilised to obtain the reduced eigenvalue problem (order $R + M + 1$) by multiplying it with matrices \mathbf{S} and \mathbf{T} from (5), (6), though it is emphasized that the integration domain is now $\Omega = D_N$:

$$(\mathbf{P}^H \mathbf{S} \mathbf{P} - k_c^2 \mathbf{P}^H \mathbf{T} \mathbf{P}) \tilde{\mathbf{v}} = \mathbf{0}, \quad (14)$$

where the superscript H refers to the Hermitian (complex conjugate transpose) operation.

It is important to note that this method yields complex eigenfunctions when $q \neq 0$ and $q \neq N/2$ if N is even. When simulating C_N structures it is desirable to skip the computation of the modes corresponding to negative values of q , since it is known they will exist and have the exact same cutoff wavenumber as their positive counterparts, and their modal electromagnetic fields will be complex conjugates. This actually means every mode of the $q \neq 0$ (and $N/2$ if N is even) family will be degenerated [28]. We offer proof that the previous assertions still hold for the proposed discretized C_N -FEM formulation in Appendix A, contrary to general-purpose FEM where known degenerate modes are split (either when solving for the whole cross-section or imposing different PMC/PEC conditions in axial symmetry planes). This implies that to obtain a complete set of modes only $\lfloor N/2 \rfloor + 1$ eigenvalue problems need to be solved with the proposed C_N -FEM, thus compensating for the need of using complex algebra to solve the cases $q \neq 0, N/2$, as only real algebra is needed for the general-purpose FEM implementation.

III. RESULTS

To validate the accuracy of the proposed C_N -FEM method, we present a handful of results from various structures with one or no symmetry planes, shown in Fig. 3. To make fair comparisons between structures and procedures some considerations are taken into account. First, the domains D_N have been normalised to have an area of 1 for all structures. Then, 20 TE and TM modes have been computed for each mode class which result in $40N$ modes in the global scheme. Lastly, to compare against general-purpose FEM [11], [12], we simulated with approximately N times the amount of DOFs for the whole structure, as this is approach reasonably takes into account the accuracy gained when using C_N -FEM. These DOFs are always real for the general-purpose FEM and complex for C_N -FEM unless the mode class $q = 0$ or $N/2$ for N even is being computed.

In each table the dimensions and number of DOFs is presented, along with the set of modes identified between brackets “ $\{i...j\}$ ” by propagation order of their mode family corresponding to their cutoff wavenumber k_c values (with dimensions of inverse of normalized length units.) For general-purpose FEM two rows labelled “A” and “B” are needed for

each C_N -FEM row since the general formulation does not guarantee identical k_c for degenerate modes. For waveguides with analytic solutions, degenerate modes have exact equal values, since their k_c are computed with a closed formula.

First, we obtained the cutoff wavenumbers for an analytical waveguide, in this case the equilateral triangular waveguide in Fig. 3(a) [29], [30], for which we show the first 2 TE modes for all mode classes and the 20th ones (to show the accuracy). The amount of DOFs was tuned to achieve a relative error of less than 0.15% for the highest-order TE mode of the class $q = 1$ with respect to the analytical solution. The results in Tables I and II show a comparison between the proposed method and the analytical solution, where the fact that the proposed C_N -FEM method is able to discriminate all the degenerate modes is evidenced.

A cross-section with an even value of N is presented in Fig 3(b), whose k_c values for TE and TM modes are shown in Tables III and IV, respectively. Note that in this structure, there are two mode families that are derived with linear polarization and do not have guaranteed degeneracy between any of their modes ($q = \{0, 2\}$). The relative difference between methods is inferior to 0.15%, which shows they have a similar convergence given a DOF count ratio proportional to N . Tables V, VI show the first TE and TM cutoff wavenumbers obtained for a pentagonal waveguide using this technique, which are compared against a classic FEM simulation of the problem using the entire cross-section, obtaining a relative difference of less than 0.1%. In all numerical cases the exact same solver was used. For simple structures such as this one, lower order modes will have very similar cutoff wavenumbers. For higher order modes this degeneracy becomes less clear as the numbers start to inevitably diverge.

To show how our model can be applied to all kinds of structures with C_N properties, we finally tested the waveguide of Fig. 1(b) with parameters given in Fig. 3(d). The results are compared against a classic cross-section simulation using the same solver. In this case $N = 7$, which allows for a reduction of the simulation area of 7 times and allows for 7 different mode classes. Results can be observed in Tables VII and VIII. It can be seen how a general-purpose FEM implementation struggles when obtaining cutoff wavenumbers for degenerate modes in complex structures. The relative difference between solutions from the two methods goes up to 0.04%. Note that in this case, because of the complexity of the structure, even lower order degenerate modes start to present disparities in their k_c .

When computing the fields using the C_N -FEM scheme it becomes very important to take into account that the obtained eigenvectors are complex for mode classes with $q \neq 0$ or $N/2$ if N is even. This, of course, has to be the case since these eigenvectors contain twice the information of the ones obtained through classic FEM. In Fig. 4, three modes are presented for different structures. The figures show the power density for some TE and TM modes with different q values.

IV. CONCLUSION

As more waveguide devices are developed using C_N schemes, the use of tailored and efficient simulation tools

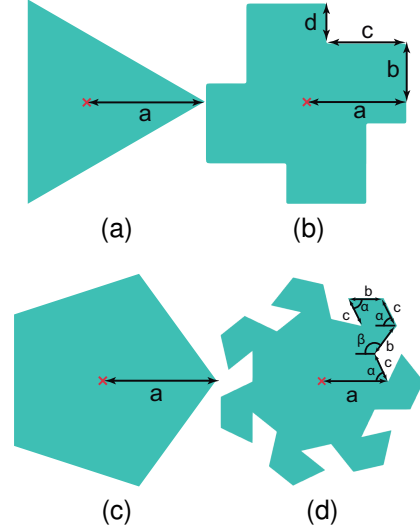


Fig. 3. C_N waveguides: (a) C_3 equilateral waveguide, (b) C_4 quadrangular waveguide, (c) C_5 pentagonal waveguide, (d) C_7 shredded waveguide.

TABLE I
 k_c VALUES FOR TE MODES IN AN EQUILATERAL TRIANGULAR WAVEGUIDE (C_3) (FIG. 3 (A), $a = 1.512$). DOFs(C_N -FEM)=485.

Mode class q	0	± 1
{1...3} (C_N -FEM)	2.7564	1.5907
A (analytic)	2.7563	1.5914
B (analytic)	n/a	same
{4...6} (C_N -FEM)	4.7743	3.1815
A (analytic)	4.7742	3.1828
B (analytic)	n/a	same
...
{58...60} (C_N -FEM)	14.3566	14.1633
A (analytic)	14.3226	14.1446
B (analytic)	n/a	same

TABLE II
 k_c VALUES FOR TM MODES IN AN EQUILATERAL TRIANGULAR WAVEGUIDE (C_3) (FIG. 3 (A), $a = 1.512$). DOFs(C_N -FEM)=485.

Mode class q	0	± 1
{1...3} (C_N -FEM)	2.7569	4.2072
A (analytic)	2.7563	4.2144
B (analytic)	n/a	same
{4...6} (C_N -FEM)	5.5130	5.7350
A (analytic)	5.5128	5.7379
B (analytic)	n/a	same
...
{58...60} (C_N -FEM)	16.8447	16.9014
A (analytic)	16.7664	16.8418
B (analytic)	n/a	same

becomes increasingly desirable. The approach that has been presented, based on rotational periodic boundary conditions, extends the PEC and PMC analysis for structures with or without axial symmetry, and has been shown to have many advantages. First, it allows for a dimensionality reduction that is more prominent the higher the value of N is, with the only overhead of establishing the rotational periodic boundary

TABLE III

k_c VALUES FOR TE MODES IN THE QUADRANGULAR STRUCTURE IN FIG. 3(B) (C_4). $a = 1.2126$, $b = 0.6a$, $c = 0.8a$, $d = 0.4a$
DOFs(C_N -FEM)=532, DOFs(FEM)=2588.

Mode class q	0	± 1	2
{1...4} (C_N -FEM)	3.0015	1.4338	1.8437
A (FEM)	3.0013	1.4339	1.8433
B (FEM)	n/a	1.4339	n/a
{5...8} (C_N -FEM)	3.8493	3.4562	3.3288
A (FEM)	3.8489	3.4564	3.3287
B (FEM)	n/a	3.4564	n/a
...
{77...80} (C_N -FEM)	14.7641	14.5099	14.7789
A (FEM)	14.7529	14.5000	14.7694
B (FEM)	n/a	14.5004	n/a

TABLE IV

k_c VALUES FOR TM MODES IN THE QUADRANGULAR STRUCTURE IN FIG. 3(B) (C_4). $a = 1.2126$, $b = 0.6a$, $c = 0.8a$, $d = 0.4a$
DOFs(C_N -FEM)=532, DOFs(FEM)=2588.

Mode class q	0	± 1	2
{1...4} (C_N -FEM)	2.5149	3.8172	4.4272
A (FEM)	2.51411	3.8176	4.4270
B (FEM)	n/a	3.8177	n/a
{5...8} (C_N -FEM)	5.0172	5.6804	5.8433
A (FEM)	5.0171	5.6816	5.8411
B (FEM)	n/a	5.6817	n/a
...
{77...80} (C_N -FEM)	16.8867	16.9245	16.9034
A (FEM)	16.8701	16.9082	16.8821
B (FEM)	n/a	16.9098	n/a

TABLE V

k_c VALUES FOR TE MODES IN A REGULAR PENTAGONAL WAVEGUIDE (C_5) (FIG. 3(C)), $a = 1.450$. DOFs(C_N -FEM)=489,
DOFs(FEM)=2521.

Mode class q	0	± 1	± 2
{1...5} (C_N -FEM)	2.9839	1.4387	2.3051
A (FEM)	4.3257	1.4390	2.3050
B (FEM)	n/a	1.4390	2.3050
{6...10} (C_N -FEM)	4.6220	3.8354	3.3819
A (FEM)	4.6216	3.8360	3.3819
B (FEM)	n/a	3.8360	3.3819
...
{96...100} (C_N -FEM)	14.7626	14.8846	14.8974
A (FEM)	14.7521	14.8879	14.8945
B (FEM)	n/a	14.8886	14.8956

TABLE VI

k_c VALUES FOR TM MODES IN A REGULAR PENTAGONAL WAVEGUIDE (C_5) (FIG. 3(C)), $a = 1.450$. DOFs(C_N -FEM)=489,
DOFs(FEM)=2521.

Mode class q	0	± 1	± 2
{1...5} (C_N -FEM)	1.9454	3.0909	4.1178
A (FEM)	1.9452	3.0921	4.1177
B (FEM)	n/a	3.0921	4.1177
{6...10} (C_N -FEM)	4.4338	5.5373	5.1468
A (FEM)	4.4325	5.5394	5.1468
B (FEM)	n/a	5.5394	5.1468
...
{96...100} (C_N -FEM)	16.1693	16.7524	16.6596
A (FEM)	16.1643	16.7595	16.6588
B (FEM)	n/a	16.7633	16.6621

TABLE VII

k_c VALUES FOR TE MODES IN THE SHREDDED WAVEGUIDE IN FIG. 1(B) (C_7) (ALSO FIG. 3(D)), $a = 1.209$, $b = 0.605$, $c = 0.525$, $\alpha = 5\pi/14$,
 $\beta = 2\pi/7$. DOFs(C_N -FEM)=525, DOFs(FEM)=3854.

Mode class q	0	± 1	± 2	± 3
{1...7} (C_N -FEM)	2.0005	1.0191	1.3418	1.4606
A (FEM)	2.0008	1.0193	1.3418	1.4606
B (FEM)	n/a	1.0194	1.3421	1.4609
{8...14} (C_N -FEM)	3.6185	2.5943	3.2819	3.9174
A (FEM)	3.6187	2.5950	3.2821	3.9174
B (FEM)	n/a	2.5955	3.2825	3.9177
...
{134...140} (C_N -FEM)	14.5967	14.2501	14.2505	14.5430
A (FEM)	14.5929	14.2447	14.2473	14.5382
B (FEM)	n/a	14.2460	14.2490	14.5405

TABLE VIII

k_c VALUES FOR TM MODES IN THE SHREDDED WAVEGUIDE IN FIG. 1(B) (C_7) (ALSO FIG. 3(D)), $a = 1.209$, $b = 0.605$, $c = 0.525$, $\alpha = 5\pi/14$,
 $\beta = 2\pi/7$. DOFs(C_N -FEM)=525, DOFs(FEM)=3854.

Mode class q	0	± 1	± 2	± 3
{1...7} (C_N -FEM)	2.0628	3.2715	4.3496	5.2627
A (FEM)	2.0644	3.2759	4.3548	5.2730
B (FEM)	n/a	3.2760	4.3549	5.2733
{8...14} (C_N -FEM)	4.6655	5.7601	6.2926	6.3043
A (FEM)	4.6714	5.7734	6.3031	6.3095
B (FEM)	n/a	5.7735	6.3039	6.3101
...
{134...140} (C_N -FEM)	16.7121	17.2747	17.3206	17.2453
A (FEM)	16.7165	17.2326	17.3149	17.2769
B (FEM)	n/a	17.2362	17.3162	17.2778

condition. Secondly, the use of the mode families categorized by their mode class q value gives mathematical proof of degeneracy for the modes with $q \neq 0$ and $N/2$ if N is even. The presented implementation guarantees the exact same cutoff wavenumber for degenerated modes. Third, the method obtains directly the modes with circular polarisation that will be used in C_N structures composed of several cascaded different C_N waveguides. This is an advantage because it gives information about how the different mode families will be propagating through the structure and predicts mode coupling behaviour, while also providing information about the fields

that will be used in polarisers and other devices designed to work with this kind of propagation.

APPENDIX A

PROOF OF DEGENERACY IN C_N -FEM BETWEEN MODES WITH $\pm q$

Proof of analytical degeneracy between modes obtained for values q and $-q$ can be found in [20]. As this result does not necessarily translate to a numerical formulation, we offer proof that the one presented in this paper also provides the same cutoff wavenumbers for $\pm q$ values and the simple, expected

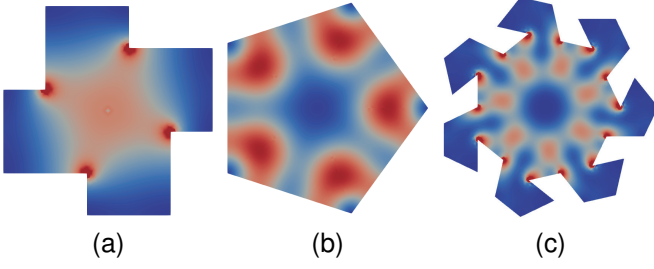


Fig. 4. Average power density of: (a) First TE mode with $q = 1$, quadrangular waveguide in Fig. 3(b); (b) Second TE of the family with $q = 2$ of the pentagonal waveguide in Fig. 3(c); (c) First TM of the family with $q = 3$ of the shredded waveguide in Fig. 3(d).

relationship between their eigenvectors. First, recalling from (11) and (12) that matrices \mathbf{P}_{ss} and \mathbf{P}_{sm} are strictly real, we establish the relationship between matrix \mathbf{P} in both cases:

$$\mathbf{P}_{-q} = \mathbf{P}_q^*, \quad \mathbf{P}_{-q}^H = (\mathbf{P}_q^*)^H = \mathbf{P}_q^T, \quad (15)$$

where superscript $*$ refers to the complex conjugate and T stands for the transpose operation. For the sake of clarity, let us define the intermediate matrices found in (14):

$$\mathbf{A}_q = \mathbf{P}_q^H \mathbf{S} \mathbf{P}_q, \quad \mathbf{B}_q = \mathbf{P}_q^H \mathbf{T} \mathbf{P}_q. \quad (16)$$

Now it is possible to rewrite (14) for both $\pm q$ cases, and then apply (15), taking into account that \mathbf{S} and \mathbf{T} in (16) always have real entries:

$$(\mathbf{A}_q - k_{c,q}^2 \mathbf{B}_q) \mathbf{v}_q = \mathbf{0}, \quad (17)$$

$$(\mathbf{A}_{-q} - k_{c,-q}^2 \mathbf{B}_{-q}) \mathbf{v}_{-q} = (\mathbf{A}_q^* - k_{c,-q}^2 \mathbf{B}_q^*) \mathbf{v}_{-q} = \mathbf{0}. \quad (18)$$

By inspection of these equations we come to the conclusion that $k_{c,q}^2 = (k_{c,-q}^2)^*$. Since matrices \mathbf{S} and \mathbf{T} are real symmetric as per (5) and (6), then \mathbf{A}_q and \mathbf{B}_q are Hermitian matrices, namely $\mathbf{A}_q = \mathbf{A}_q^H$, $\mathbf{B}_q = \mathbf{B}_q^H$. This implies both eigenvalues are identical since the mathematical solution of generalized Hermitian eigenvalue problems can only be real. Finally we apply this result to (18) and obtain

$$(\mathbf{A}_{-q} - k_{c,-q}^2 \mathbf{B}_{-q}) \mathbf{v}_{-q} = (\mathbf{A}_q - k_{c,q}^2 \mathbf{B}_q)^* \mathbf{v}_{-q} = \mathbf{0}. \quad (19)$$

Comparing this result to (17) yields $\mathbf{v}_{-q} = \mathbf{v}_q^*$, which shows that the eigenvectors are to be complex conjugates. This means the analytical result for analytical C_N modes is maintained in the proposed numerical implementation.

REFERENCES

- [1] O. Zetterstrom, G. Valerio, F. Mesa, F. Ghasemifard, M. Norgren, and O. Quevedo-Teruel, "Mode-matching analysis of loaded transmission lines with twist symmetries," *EurAAP*, 2020, pp. 1–5.
- [2] N. Kolmakova, S. Prikolotin, A. Perov, V. Derkach, and A. A. Kirilenko, "Polarization plane rotation by arbitrary angle using D-4 symmetrical structures," *IEEE Trans. Microw. Theory Tech.*, vol. 64, no. 2, pp. 429–435, 2016.
- [3] M. Bagheriasl, O. Quevedo-Teruel, and G. Valerio, "Bloch analysis of artificial lines and surfaces exhibiting glide symmetry," *IEEE Trans. Microw. Theory Tech.*, vol. 67, no. 7, pp. 2618–2628, 2019.
- [4] M. Bagheriasl and G. Valerio, "Bloch analysis of electromagnetic waves in twist-symmetric lines," *Symmetry*, vol. 11, no. 5, 2019.
- [5] P. R. McIsaac, "Symmetry-induced modal characteristics of uniform waveguides," in *S-MTT International Microwave Symposium Digest*, vol. 74, no. 1, 1974, pp. 75–77.

- [6] G. Conciauro, *Advanced modal analysis : CAD techniques for waveguide components and filters*. John Wiley & Sons, 2000.
- [7] J. Córcoles, A. Morán-López, and J. A. Ruiz-Cruz, "Nested 2D finite-element function-spaces formulation for the mode-matching problem of arbitrary cross-section waveguide devices," *Applied Mathematical Modelling*, vol. 60, pp. 286–299, 2018.
- [8] L. Polo-López, J. Córcoles, J. A. Ruiz-Cruz, J. R. Montejó-Garai, and J. M. Rebollar, "On the theoretical maximum directivity of a radiating aperture from modal field expansions," *IEEE Trans. Antennas Propag.*, vol. 67, no. 4, pp. 2781–2786, 2019.
- [9] F. L. Ng, "Tabulation of methods for the numerical solution of the hollow waveguide problem (short papers)," *IEEE Trans. Microw. Theory Tech.*, vol. 22, no. 3, pp. 322–329, 1974.
- [10] S. Saad, "Review of numerical methods for the analysis of arbitrarily-shaped microwave and optical dielectric waveguides," *IEEE Trans. Microw. Theory Tech.*, vol. 33, no. 10, pp. 894–899, 1985.
- [11] G. Pelosi, R. Coccioli, and S. Selleri, *Quick Finite Elements for Electromagnetic Waves*, ser. Artech House electromagnetic analysis series. Artech House, 2009.
- [12] J. Jin, *The Finite Element Method in Electromagnetics*, ser. Wiley - IEEE. Wiley, 2015.
- [13] R. Sorrentino and T. Itoh, "Transverse resonance analysis of finline discontinuities," *IEEE Trans. Microw. Theory Tech.*, vol. 32, no. 12, pp. 1633–1638, 1984.
- [14] G. Conciauro, M. Bressan, and C. Zuffada, "Waveguide modes via an integral equation leading to a linear matrix eigenvalue problem," *IEEE Trans. Microw. Theory Tech.*, vol. 32, no. 11, pp. 1495–1504, 1984.
- [15] E. Kühn, "A contour-integral matching method for the analysis of metallic and dielectric waveguides of arbitrary cross-section," *Archiv Elektronik und Uebertragungstechnik*, vol. 40, pp. 263–270, Oct. 1986.
- [16] F. Giese, J. Reiter, and F. Arndt, "Modal analysis of arbitrarily shaped irises in waveguides by a hybrid contour-integral mode-matching method," in *Proceedings of 1995 IEEE MTT-S International Microwave Symposium*. IEEE, 1995, pp. 1359–1362 vol.3.
- [17] J. A. Ruiz-Cruz and J. M. Rebollar, "Eigenmodes of waveguides using a boundary contour mode-matching method with an FFT scheme," *Int. J. RF Microw. Comput.-Aid. Eng.*, vol. 15, no. 3, pp. 286–295, 2005.
- [18] B. Deutschmann and A. F. Jacob, "Broadband septum polarizer with triangular common port," *IEEE Trans. Microw. Theory Tech.*, vol. 68, no. 2, pp. 693–700, 2020.
- [19] P. R. McIsaac, "Symmetry-induced modal characteristics of uniform waveguides - II: Theory," *IEEE Trans. Microw. Theory Tech.*, vol. 23, no. 5, pp. 429–433, 1975.
- [20] S. V. Silin R.A., *Slow-down Systems*. Soviet Radio, 1966.
- [21] A. A. Kirilenko, N. G. Kolmakova, and S. A. Prikolotin, "Ultra-compact 90deg twist based on a pair of two closely placed flat chiral irises," *Radioelectronics and Communications Systems*, vol. 55, no. 4, pp. 175–177, 2012.
- [22] N. Kolmakova, S. Prikolotin, A. Kirilenko, and A. Perov, "Simple example of polarization plane rotation by the fringing fields interaction," in *2013 European Microwave Conference*, 2013, pp. 936–938.
- [23] A. A. Kirilenko, S. O. Steshenko, V. N. Derkach, and Y. M. Ostryzhnyi, "A tunable compact polarizer in a circular waveguide," *IEEE Trans. Microw. Theory Tech.*, vol. 67, no. 2, pp. 592–596, 2019.
- [24] D. Pozar, *Microwave Engineering*. Wiley, 2011.
- [25] R. E. Collin, *Foundations for microwave engineering*, ser. McGraw-Hill physical and quantum electronics series. New York: McGraw-Hill, 1966.
- [26] A. A. Tavallae and J. P. Webb, "Finite-element modeling of evanescent modes in the stopband of periodic structures," *IEEE Trans. Magn.*, vol. 44, no. 6, pp. 1358–1361, 2008.
- [27] A. Bostani and J. P. Webb, "Finite-element eigenvalue analysis of propagating and evanescent modes in 3-D periodic structures using model-order reduction," *IEEE Trans. Microw. Theory Tech.*, vol. 60, no. 9, pp. 2677–2683, 2012.
- [28] M. Mrozowski, *Guided Electromagnetic Waves: Properties and Analysis*, ser. Computer methods in electromagnetics series. Research Studies Press, 1997.
- [29] B. J. McCartin, "Eigenstructure of the equilateral triangle, part II: The Neumann problem," *Mathematical problems in engineering*, vol. 2002, no. 6, pp. 517–539, 2002.
- [30] —, "Eigenstructure of the equilateral triangle, part I: The Dirichlet problem," *SIAM review*, vol. 45, no. 2, pp. 267–287, 2003.